



**Controllable generation of several nonlinear waves in optical fibers with third-order dispersion**Peng Gao,<sup>1,2</sup> Liang Duan<sup>3</sup>,, Xiankun Yao,<sup>1,2,4</sup> Zhan-Ying Yang<sup>1,2,4,\*</sup>, and Wen-Li Yang<sup>1,2,4,5</sup><sup>1</sup>*School of Physics, Northwest University, 710127 Xi'an, China*<sup>2</sup>*Shaanxi Key Laboratory for Theoretical Physics Frontiers, 710127 Xi'an, China*<sup>3</sup>*School of Physics and Astronomy, Shanghai Jiao Tong University, 200240 Shanghai, China*<sup>4</sup>*Peng Huanwu Center for Fundamental Theory, 710127 Xi'an, China*<sup>5</sup>*Institute of Modern Physics, Northwest University, 710127 Xi'an, China*

(Received 30 November 2020; accepted 29 January 2021; published 15 February 2021)

We propose a method to controllably generate six kinds of nonlinear waves on continuous waves, including the one- and multi-peak solitons, the Akhmediev, Kuznetsov-Ma, and Tajiri-Watanabe breathers, and stable periodic waves. In the nonlinear fiber system with third-order dispersion, we illustrate their generation conditions by the modified linear stability analysis and numerically generate them from initial perturbations on continuous waves. We implement the quantitative control over their dynamical features, including the wave type, velocity, periodicity, and localization. Our results may provide an effective scheme for generating optical solitons on continuous waves, and it can also be applied for wave generations in other various nonlinear systems.

DOI: [10.1103/PhysRevA.103.023519](https://doi.org/10.1103/PhysRevA.103.023519)**I. INTRODUCTION**

Nonlinear wave generation has recently become a subject of intense research in optical fiber systems. Successful generation of some fundamental waves was implemented, such as soliton [1–6], breathers [7–10], and Peregrine rogue wave [11,12]. It benefits from the research on the wave's exact solutions and generation mechanisms in the nonlinear Schrödinger (NLS) model [13–22]. This famous model describes the propagation of optical pulse in a nonlinear fiber without high-order effects and is also remarkably effective for other diverse physical systems [23–27].

For an ultrashort pulse, some high-order effects need to be introduced into the NLS model to ensure its effectiveness [23]. When the coefficients of introduced effects exhibit some proportions, the model is still integrable, such as the Hirota [28] and Sasa-Satsuma [29] models, etc. [30]. In these models, more kinds of nonlinear waves were presented in the form of exact solutions (especially the waves on continuous waves), like one- and multi-peak solitons and periodic waves [31–40]. Although the complexity of these models makes their realization in real fibers difficult, the exact solutions of nonlinear waves undoubtedly enrich the types of wave patterns and provide new potential applications of wave generation.

The key point is how to achieve and control the generation of these waves in real fibers. To this end, some efforts have been made to study their generation mechanism. Successful controls on the generations of Akhmediev breathers and Peregrine rogue waves have been given by the standard linear stability analysis (LSA) [7,41]. They originate from the modulation instability of periodic and localized perturbations, respectively. However, the controllable generations of

other waves need more feature parameters besides instability gain, especially their periodicity and localization [42,43]. It prompts us to focus on the modified LSA [44]. This method was presented to predict the quantitative dynamics of a perturbed continuous wave, including the periodicity and localization of generated waves. Thus, it provides the possibility to control wave generation in real nonlinear fibers.

In this paper, we analyze the wave features under different parameters by the modified LSA, including the periodicity, localization, and velocities of waves. We classify the six kinds of waves on continuous waves according to their features and illustrate their several generation conditions. These mechanisms of wave generation are implemented in the NLS models with third-order dispersion, and we achieve the control over their types and features. Third-order dispersion plays a key role in enriching the types of generated waves, like the multi- and one-peak solitons on continuous waves. Then, the experimental feasibility of multi- and one-peak soliton generation is verified under the parameters of a genuine nonlinear fiber. The impact of Raman scattering on wave generation is also discussed.

**II. MODIFIED LINEAR STABILITY ANALYSIS FOR WAVE FEATURES**

The optical field in a nonlinear fiber can be described by the NLS equation. Considering third-order dispersion, its dimensionless model with abnormal group-velocity dispersion is denoted [23]

$$i\psi_z + \frac{1}{2}\psi_{tt} - \frac{i\beta_3}{6}\psi_{ttt} + |\psi|^2\psi = 0, \quad (1)$$

where  $\psi(z, t)$  represents the slowly varying complex envelope of optical field,  $z, t$  are respectively the evolution distance and retarded time, and the subscripts  $z$  and  $t$  denote the partial

\*zyyang@nwu.edu.cn

derivative of the variable with respect to them in this paper.  $\beta_3$  corresponds to the third-order dispersion. Although the generation conditions of some waves have been given in some integrable models with high-order effects, difficulties still remains for nonintegrable systems, such as Eq. (1).

To realize their generations, we try an initial condition with the form of

$$\begin{aligned}\psi_p(0, t) &= [1 + u(0, t)]\psi_0(0, t) \\ &= [1 + (a_1 e^{i\omega_p t} + a_2 e^{-i\omega_p t})L(t)]a_0 e^{i\omega_0 t}.\end{aligned}\quad (2)$$

The initial continuous-wave background  $\psi_0(0, t)$  has its amplitude  $a_0$  and frequency  $\omega_0$ . The initial perturbation  $u(0, t)$  has a localized envelope  $L(t)$  and the modulated periodic wave with double frequencies  $\omega_p$  and  $-\omega_p$ , whose amplitudes are  $a_1$  and  $a_2$  (here we assume  $\omega_p > 0$ ). The two-frequency form of periodic waves provides convenience for feature analysis of the perturbing wave. Besides,  $L(t)$  is a smooth localized function whose limit values at  $|t| \rightarrow \infty$  are zero. Here, we consider  $L(t) = \text{sech}(\eta_p t)$ , where  $\eta_p > 0$  scales the localization of this function. There were many studies in integrable models showing that sech-type initial perturbations can generate fundamental waves with more standard patterns than those with other types of envelopes [43,45–47].

Now we start the analysis on dynamical features of the perturbing wave. A perturbed continuous wave is assumed as

$$\psi_p(z, t) = [1 + u(z, t)]\psi_0(z, t).\quad (3)$$

Here,  $\psi_0(z, t)$  is a continuous-wave solution of Eq. (1) with the form  $\psi_0(z, t) = a_0 \exp(i\omega_0 t - ik_0 z)$ , where  $a_0$ ,  $\omega_0$ , and  $k_0$  are the amplitude, frequency, and propagating constant of background wave, respectively, and  $k_0 = -a_0^2 + \omega_0^2/2 + \beta_3 \omega_0^3/6$ .  $u(z, t)$  stands for a weak perturbing wave with the condition  $|u|^2 \ll 1$ . Substituting Eq. (3) into the model (1), this condition allows us to figure out the linear equation about perturbing wave  $u(z, t)$ :

$$\begin{aligned}0 &= iu_z + a_0^2 u + a_0^2 u^* + \left(i\omega_0 + \frac{i\beta_3}{2}\omega_0^2\right)u_t \\ &\quad + \left(\frac{1}{2} + \frac{\beta_3}{2}\omega_0\right)u_{tt} + \left(-\frac{i\beta_3}{6}\right)u_{ttt}.\end{aligned}\quad (4)$$

We consider a perturbing wave of the form

$$u(z, t) = A e^{p(z,t)} + B e^{p^*(z,t)}.\quad (5)$$

where  $p(z, t)$  is a complex function about coordinates with a general form.  $A$  and  $B$  are the amplitudes of two conjugate components whose initial values are equal to  $a_1$  and  $a_2$ , respectively. Our method is applicable only when  $A$  and  $B$  are small quantities in principle, due to the condition  $|u|^2 \ll 1$ . However, in our some numerical simulations, their moderate values compared with background amplitude also admit our control over the wave's features. To observe the obvious wave generation, we try to set initial perturbations comparable with the background wave, which will be illustrated in Sec. IV. We substitute Eq. (5) into Eq. (4) and obtain a set of two homogeneous equations for  $a_1$  and  $a_2^*$ . This set has a nontrivial solution only when the determinant of the coefficient matrix

is equal to zero. Thus, the expression of  $p_z$  is

$$p_z = -\omega_0 p_t + \frac{1}{6}\beta_3 N \pm \frac{1}{2}\sqrt{M(4a_0^2 - M)},\quad (6)$$

where  $M = -(p_t^2 + p_{tt})(1 + \beta_3 \omega_0)$  and  $N = p_t^3 + p_{ttt} + 3p_t p_{tt} - 3\omega_0^2 p_t$ . Comparing Eq. (5) with Eq. (2), one can obtain that  $p(0, t) = i\omega_p t + \ln L(t) = i\omega_p t + \ln[\text{sech}(\eta_p t)]$ . It indicates that, at the initial distance  $z = 0$ ,  $p_t = i\omega_p + L_t/L$ ,  $p_{tt} = (-L_t^2 + LL_{tt})/L^2$ ,  $p_{ttt} = (2L_t^3 - 3LL_t L_{tt} + L^2 L_{ttt})/L^3$ , which can be substituted into Eq. (6) for the specific expression of  $p_z$ .

The wave's frequency and propagation constant can be represented by the rate of change of phase  $\text{Im}[p]$  with  $t$  and  $z$ , respectively,

$$\omega = \text{Im}[p_t], \quad K = -\text{Im}[p_z].\quad (7)$$

They scale the wave's periodicity in the  $t$  and  $z$  directions. Considering that the shape of the wave envelope is related to the real part of  $p$ , one can describe the wave's localization in the  $t$  and  $z$  directions by the rate of change of  $\text{Re}[p]$ , namely,

$$\eta = \text{Re}[p_t], \quad G = -\text{Re}[p_z].\quad (8)$$

Meanwhile, the periodicity manifests itself as interference fringes formed by the interaction between background and perturbing waves; the localization manifests itself as a localized envelope on a background wave. We can respectively give the velocities of fringe and localized envelope,

$$V = K/\omega, \quad \Lambda = G/\eta.\quad (9)$$

Up to now, the wave's periodicity, localization, and velocities are described by the above six functions about  $t$ , but they are not convenient to adjust to the features of the wave. Thus, we consider the relationship between  $\eta_p$  and  $\eta$ :

$$\lim_{t \rightarrow \pm\infty} \eta = \mp \eta_p.\quad (10)$$

It indicates that the localization of the wave envelope can be described precisely by the limit of the function  $\eta$  when  $t$  approaches positive or negative infinity. Therefore, we introduce a subscript (+ or -) of the function  $f$  to denote its limit value when  $t \rightarrow +\infty$  or  $t \rightarrow -\infty$ :

$$f_{\pm} = \lim_{t \rightarrow \pm\infty} f.$$

It provides convenient limit values to depict the six features mentioned above, namely,  $\omega_{\pm}$ ,  $\eta_{\pm}$ ,  $K_{\pm}$ ,  $G_{\pm}$ ,  $V_{\pm}$ , and  $\Lambda_{\pm}$ . For the initial condition (2), we have  $\omega_+ = \omega_- = \omega_p$  and  $\eta_+ = -\eta_- = -\eta_p$ . We usually also have  $K_+ = K_-$  and  $G_+ = -G_-$  in our used model (1), which leads to  $V_+ = V_-$  and  $\Lambda_+ = \Lambda_-$  (except for the generation of one-peak soliton mentioned below). Meanwhile, to make  $V_{\pm}$  and  $\Lambda_{\pm}$  describe more accurately the propagation of the whole wave, the distributions of  $V$  and  $\Lambda$  on  $t$  need to be approximately constant. It requires that the envelope of the initial perturbation be weakly localized, namely,  $\eta_p < 1$ .

There exists an important problem:  $p_z$  in Eq. (6) is a multivalued complex function and so has two branches on its Riemann surfaces,  $p_z^{B+}$  and  $p_z^{B-}$ , which indicates that the limit values of above six functions when  $t \rightarrow +\infty$  and  $t \rightarrow -\infty$  may locate on different branches. For an example, when  $\beta_3 = 0.1$ ,  $\eta_p = 0.5$ ,  $a_0 = 1$ , and  $\omega_0 = 0$ , the Riemann surfaces of

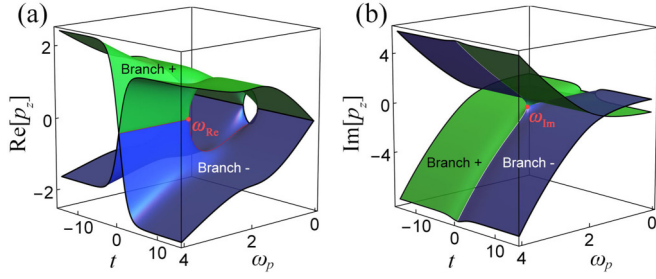


FIG. 1. Riemann surfaces of (a)  $\text{Re}[p_z]$  and (b)  $\text{Im}[p_z]$  with respect to  $t$  and  $\omega_p$ . Branches + (green surface) and - (blue surface) respectively denote the function  $p_z$  with + and - before the square-root sign. The branches of  $\text{Re}[p_z]$  (or  $\text{Im}[p_z]$ ) are not continuous about  $t$  when  $\omega_p > \omega_{\text{Re}}$  (or  $\omega_p > \omega_{\text{Im}}$ ). The parameters are set as  $\beta_3 = 0.1$ ,  $\eta_p = 0.5$ ,  $a_0 = 1$ , and  $\omega_0 = 0$ .

$\text{Re}[p_z]$  and  $\text{Im}[p_z]$  with respect to  $t$  and  $\omega_p$  are shown in Fig. 1. The green or blue surfaces respectively denote the branches when the sign before the square-root sign in Eq. (6) is + or -, called branch + or branch - here. In Fig. 1(a), there is a red cross line between branches + and -, and this line ends when  $\omega_p = \omega_{\text{Re}}$ . In the case of  $\omega_p > \omega_{\text{Re}}$ , the two branches are not continuous at  $t = 0$ , so one needs to change the branch for its limit values at  $t \rightarrow +\infty$  and  $t \rightarrow -\infty$ . In the case of  $\omega_p < \omega_{\text{Re}}$ , the cross line disappears so the branch is not changed. Similarly, Fig. 1(b) shows the point where the cross line between the two branches ends, assumed as  $\omega_{\text{Im}}$ . The continuity about  $t$  remains in the range  $\omega_p < \omega_{\text{Im}}$  and disappears when  $\omega_p > \omega_{\text{Im}}$ . To distinguish the two classes of results from two different continuous surfaces, we call the waves on branch + when  $t \rightarrow +\infty$  “mode I,” and those on branch - when  $t \rightarrow +\infty$  “mode II.” They are respectively denoted by the superscripts (I) and (II). The relation between the modes and branches is shown in Table I. Note that this relation is applicable under the parameters in our example, which demonstrates an example of how to deal with different branches. The cases with other parameters may admit various distributions of branches and so require recalculations of the relations.

As different modes can admit different dynamical features of perturbing waves, it is necessary to implement the choice of mode. The mode choice can be realized by setting different initial amplitudes of perturbation  $A$  and  $B$ . With a small  $B$ , one can obtain the required  $A$  from the homogeneous equation set,

$$A^{(\text{I,II})} = a_0^2 B^* / \left[ -i\omega_0 p_t + \frac{i}{6}\beta_3 N + \frac{1}{2}M - ip_z^{(\text{I,II})} - a_0^2 \right]. \quad (11)$$

TABLE I. An example relation between the modes and branches.

Cases	Mode I	Mode II
$\omega_p < \omega_{\text{Re}}$	$\text{Re}[p_z]_{\pm}^{(\text{I})} = \text{Re}[p_z]_{\pm}^{\text{B}\pm}$	$\text{Re}[p_z]_{\pm}^{(\text{II})} = \text{Re}[p_z]_{\pm}^{\text{B}\mp}$
$\omega_p > \omega_{\text{Re}}$	$\text{Re}[p_z]_{\pm}^{(\text{I})} = \text{Re}[p_z]_{\pm}^{\text{B}\pm}$	$\text{Re}[p_z]_{\pm}^{(\text{II})} = \text{Re}[p_z]_{\pm}^{\text{B}\mp}$
$\omega_p < \omega_{\text{Im}}$	$\text{Im}[p_z]_{\pm}^{(\text{I})} = \text{Im}[p_z]_{\pm}^{\text{B}\pm}$	$\text{Im}[p_z]_{\pm}^{(\text{II})} = \text{Im}[p_z]_{\pm}^{\text{B}\mp}$
$\omega_p > \omega_{\text{Im}}$	$\text{Im}[p_z]_{\pm}^{(\text{I})} = \text{Im}[p_z]_{\pm}^{\text{B}\pm}$	$\text{Im}[p_z]_{\pm}^{(\text{II})} = \text{Im}[p_z]_{\pm}^{\text{B}\mp}$

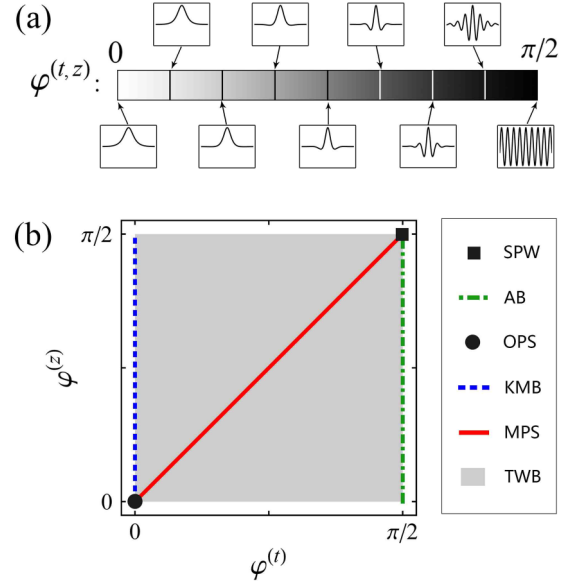


FIG. 2. (a) Typical amplitude profiles at  $t$  or  $z$  directions when  $\varphi^{(t)}$  or  $\varphi^{(z)}$  is set as different values. The localization dominates with  $\varphi^{(t,z)}$  close to 0 while the periodicity dominates with  $\varphi^{(t,z)}$  close to  $\pi/2$ . (b) Feature conditions of the six kinds of waves on  $\varphi^{(t)}$ - $\varphi^{(z)}$  plane. The black square, green dotted dashed line, black circle, blue dashed line, red solid line, and gray regions denote the conditions of SPW, AB, OPS, KMB, MPS, and TWB, respectively.

We know that  $A^{(\text{I,II})}$  is a function with respect to  $t$  and could have different limit values when  $t \rightarrow +\infty$  and  $t \rightarrow -\infty$ . From our experience, we need to average the values of  $A_+^{(\text{I,II})}$  and  $A_-^{(\text{I,II})}$ , namely,

$$A_{\text{ini}}^{(\text{I,II})} = \frac{1}{2} [A_+^{(\text{I,II})} + A_-^{(\text{I,II})}]. \quad (12)$$

It provides the required initial values of  $A$  (namely  $a_1$ ) when we generate nonlinear waves corresponding to mode I or II.

By adjusting  $\omega_p$ ,  $\eta_p$ ,  $a_0$ ,  $\omega_0$ , and  $\beta_3$ , the type, periodicity, localization, and velocities of the generated wave can be controlled. To control the types of waves, we classify the fundamental nonlinear waves by the above six features in the next section, and for convenience the superscript (I,II) will be omitted for a while.

### III. NONLINEAR WAVES AND THEIR GENERATION CONDITIONS

Periodicity and localization of perturbing waves in  $t$  or  $z$  directions can be used to classify them, and we take the case of  $t \rightarrow +\infty$  as an example here. For a wave with the periodicity ( $\omega_+$ ,  $K_+$ ) and the localization ( $\eta_+$ ,  $G_+$ ), we define two quantities,

$$\varphi^{(t)} = \tan^{-1} \left[ \frac{|\omega_+|}{|\eta_+|} \right], \quad \varphi^{(z)} = \tan^{-1} \left[ \frac{|K_+|}{|G_+|} \right]. \quad (13)$$

Both of the two quantities have the range  $0 \leq \varphi^{(t,z)} \leq \pi/2$  and they describe, respectively, the mixture of periodicity and localization in the  $t$  and  $z$  directions. In the  $t$  or  $z$  direction, the typical wave profiles corresponding to different values of  $\varphi^{(t,z)}$  are shown in Fig. 2(a). There are three types of wave

profiles: when  $\varphi^{(t,z)} = 0$ , the wave is purely localized; when  $\varphi^{(t,z)} = \pi/2$ , the wave is purely periodic; when  $0 < \varphi^{(t,z)} < \pi/2$ , the wave is periodic-localized. With the increase of  $\varphi^{(t,z)}$ , the wave's periodicity becomes strong and the localization gradually weakens. The three types can help us to classify the fundamental waves.

Their classification has been discussed in some integrable models with high-order effects [37,39,42]. Here, we slightly change it and classify them into six kinds of waves, whose feature conditions are shown in Fig. 2(b). The six waves are discussed below.

i. Stable periodic wave (SPW) is purely periodic in both the  $t$  and  $z$  directions, namely,  $\varphi^{(t)} = \varphi^{(z)} = \pi/2$ .

ii. Akhmediev breather (AB) is purely periodic in the  $t$  direction and is not purely periodic in the  $z$  direction, namely,  $\varphi^{(t)} = \pi/2$  and  $\varphi^{(z)} \neq \pi/2$ .

iii. One-peak soliton (OPS) is purely localized in both the  $t$  and  $z$  directions, namely,  $\varphi^{(t)} = \varphi^{(z)} = 0$ .

iv. Kuznetsov-Ma breather (KMB) is purely localized in the  $t$  direction and is not purely localized in the  $z$  direction, namely,  $\varphi^{(t)} = 0$  and  $\varphi^{(z)} \neq 0$ .

v. Multipeak soliton (MPS) is periodic-localized in both the  $t$  and  $z$  directions. It requires that the velocities of the fringe and localized envelope are the same, i.e.,  $V_+ = \Lambda_+$ , to make the wave shape stable in the evolution process. This condition of velocity matching is equivalent to  $\varphi^{(t)} = \varphi^{(z)}$ .

vi. Tajiri-Watanabe breather (TWB) is periodic-localized in the  $t$  direction. To ensure the existence of breathing behavior, the velocity matching needs to be avoided, namely,  $V_+ \neq \Lambda_+$ . It is equivalent to  $\varphi^{(t)} \neq \varphi^{(z)}$ .

Note that the Peregrine rogue wave is not within the scope of our discussion though it has double localization in the  $t$  and  $z$  directions. It is because a rogue wave is a special wave as the limit of breathers at  $\omega_+, \eta_+, K_+, G_+ \rightarrow 0$ , and this limit operation leads to a rational form of waves, which cannot be described by our assumed perturbing wave with exponential form. In a similar way, doubly periodic wave generation cannot be analyzed by our method due to its complex elliptic form. Besides, the above feature conditions of waves are based on the analysis of periodicity and localization, which is helpful for the wave classification. It neglects the waves with some special features, namely, the SPW with  $V_+ = 0$ , the OPS with  $\Lambda_+ = 0$ , the MPS and TWB with  $V_+ = 0$  or  $\Lambda_+ = 0$ . These neglected waves will be considered in the following discussion about the generation conditions of waves.

Let us transform the feature conditions of the six waves into their generation conditions. The generation conditions are decided by  $\omega_+, K_+, \eta_+, G_+, V_+$ , and  $\Lambda_+$  to control the type and features of generated wave and are shown in Table II. SPW and AB can be generated from a purely periodic initial perturbation (namely  $\omega_p \neq 0$  and  $\eta_p = 0$ ), generations of which can be distinguished by whether localization exists in the  $z$  direction. In similar ways, OPS and KMB can be generated from a purely localized initial perturbation (namely  $\omega_p = 0$  and  $\eta_p \neq 0$ ), generations of which can be distinguished by whether periodicity exists in the  $z$  direction; MPS and TWB can be generated from a localized-periodic initial perturbation (namely  $\omega_p \neq 0$  and  $\eta_p \neq 0$ ), generations of which can be distinguished by whether fringes a localized envelope have

TABLE II. Generation conditions of fundamental waves.

Fundamental waves	Generation conditions
Stable periodic wave (SPW)	$\omega_+ \neq 0, \eta_+ = 0, G_+ = 0$
Akhmediev breather (AB)	$\omega_+ \neq 0, \eta_+ = 0, G_+ \neq 0$
One-peak soliton (OPS)	$\omega_+ = 0, \eta_+ \neq 0, K_+ = 0$
Kuznetsov-Ma breather (KMB)	$\omega_+ = 0, \eta_+ \neq 0, K_+ \neq 0$
Multi-peak soliton (MPS)	$\omega_+ \neq 0, \eta_+ \neq 0, V_+ = \Lambda_+$
Tajiri-Watanabe breather (TWB)	$\omega_+ \neq 0, \eta_+ \neq 0, V_+ \neq \Lambda_+$

identical velocity. According to these generation conditions, the controllable generations of waves in the fiber system will be discussed in the next section.

#### IV. CONTROLLABLE GENERATION OF NONLINEAR WAVES

When  $\beta_3 = 0$ , Eq. (1) is the NLS system without the third-order dispersion. Since this system is integrable, many exact solutions describing fundamental nonlinear waves were presented [13–17]. Among the six kinds of fundamental waves mentioned above, only AB, KMB, and TWB solutions exist in NLS systems. It indicates that one can use a temporal profile as initial condition to generate them. Unlike it, what we focus on in this paper is how to controllably generate them from an initial condition with a general form, which is more convenient to prepare. In our analysis on the NLS system, the expressions of  $K_{\pm}$  and  $G_{\pm}$  are found to be wonderfully equivalent to the coefficients describing periodicity and localization in  $z$  direction given by the exact solutions of waves (which is also found in some other integrable models). This equivalence may be related to the functional form of perturbing wave solution we assume, as it can be considered as an approximate solution of initial stage in the NLS model.

Considering that many waves in the NLS model have been excited in real fibers, we focus on the system with third-order dispersion, which admits more kinds of wave generation mechanisms. Without loss of generality, the coefficient  $\beta_3$  is set as 0.1, and the background amplitude is  $a_0 = 1$ . We take mode II when  $t \rightarrow +\infty$  as an example to discuss the wave generations from three types of initial perturbations.

First, a purely periodic initial perturbation (with  $\omega_p \neq 0$  and  $\eta_p = 0$ ) is used to generate SPW or AB. When  $\eta_p = 0$ , based on Eq. (8), one can obtain

$$G_+^{(II)} = \frac{1}{2} \text{Re} \left[ \sqrt{\omega_p^2 (1 + \beta_3 \omega_0) [4a_0^2 - \omega_p^2 (1 + \beta_3 \omega_0)]} \right]. \quad (14)$$

The value of  $|G_+^{(II)}|$  is distributed on the  $\omega_0$ - $\omega$  plane to distinguish the generations of AB and SPW, as shown in Fig. 3(a1). The white ( $|G_+^{(II)}| = 0$ ) and colored ( $|G_+^{(II)}| \neq 0$ ) regions denote the generations of SPW and AB, respectively. We set the parameters as the coordinates of triangle, namely,  $(\omega_0, \omega_p) = (4, 4)$ . Its amplitude evolution is shown in Fig. 3(a2). A SPW is generated perfectly, and its velocity of fringe matches well with the one predicted by the limit value of Eq. (9) (denoted by the red dashed line). Then, we set  $(\omega_0, \omega_p) = (4, 1)$ , which

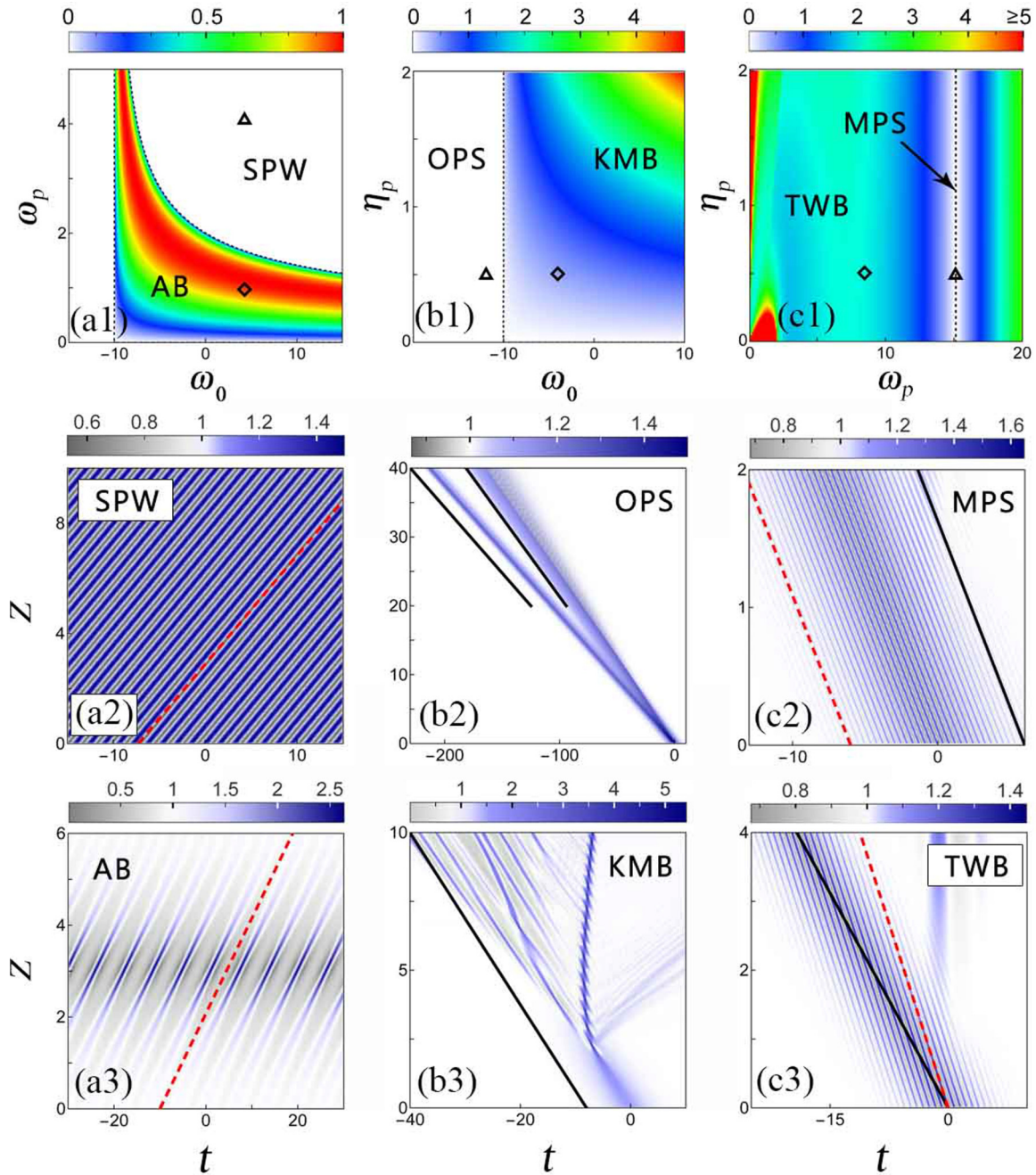


FIG. 3. (a1)  $|G_+^{(II)}|$  value distribution on  $\omega_0$ - $\omega_p$  plane with  $\eta_p = 0$ , where white and colored regions severally denote SPW and AB generations. (b1)  $|K_+^{(II)}|$  value distribution on  $\omega_0$ - $\eta_p$  plane with  $\omega_p = 0$ , where white and colored regions denote OPS and KMB generation, respectively. (c1)  $|V_+^{(II)} - \Lambda_+^{(II)}|$  value distribution on  $\omega_p$ - $\eta_p$  plane with  $\omega_0 = 0$ , where white and colored regions denote MPS and TWB generation, respectively. The middle and lower plots illustrate amplitude evolution for generating (a2) SPW, (a3) AB, (b2) OPS, (b3) KMB, (c2) MPS, and (c3) TWB. Their initial parameters are set as the coordinates of triangles or diamonds in different regions of panels (a1), (b1), and (c1). Black solid and red dashed lines represent the predicted propagating velocities of the localized envelope and fringe, respectively. All the waves are generated successfully, except the KMB. The splitting in OPS generation is related to the nondegeneracy of modes and time signs. Other parameters are  $\beta_3 = 0.1$  and  $a_0 = 1$ .

are the coordinates of the diamond in Fig. 3(a1). Its amplitude evolution is shown in Fig. 3(a3), and an AB is generated as expected. Its numerical velocity of the fringe also agrees well with the one we predict.

Second, we consider a purely localized initial perturbation (with  $\omega_p = 0$  and  $\eta_p \neq 0$ ) to generate OPS or KMB. When

$\omega_p = 0$ , based on Eq. (7), one can obtain

$$K_+^{(II)} = \frac{1}{2} \text{Im} \left[ \sqrt{-\eta_p^2 (1 + \beta_3 \omega_0) [4a_0^2 + \eta_p^2 (1 + \beta_3 \omega_0)]} \right]. \quad (15)$$

The distribution of  $|K_+^{(II)}|$  on the  $\omega_0$ - $\eta_p$  plane is shown in Fig. 3(b1) for their generation conditions. Unlike the NLS

system, the consideration of third-order dispersion admits the OPS generation, which is denoted by the gray region (with  $|K_+^{(II)}| = 0$ ). The colored region (with  $|K_+^{(II)}| \neq 0$ ) corresponds to KMB generation. For a purely localized initial perturbation, its initial condition (2) becomes

$$\psi_{loc}(0, t) = [1 + (A + B)\text{sech}(\eta_p t)]a_0 e^{i\omega_0 t}. \quad (16)$$

It indicates that the generation mode cannot be selected by the combinations of different  $A$  and  $B$ . We set the total amplitude  $A + B$  as the modest value of 0.5 to try to generate KMB or OPS. We set  $(\omega_0, \eta_p)$  as the triangle's coordinates  $(-12, 0.5)$ , and the amplitude evolution plot is shown in Fig. 3(b2). The initial localized envelope splits into to waves with different velocities. The left-hand wave has a stable shape in the propagation process, so we consider it as an OPS. The right-hand wave gets wider and wider with the increasing distance, and it has a typical shape of dispersive shock wave. Compared with our analysis result, the wave splitting indicates the generation of nondegenerate waves for different modes and time signs. The velocities of two waves need to be predicted by  $\Lambda_+^{(II)}$  and  $\Lambda_-^{(II)}$ , which are shown in Fig. 3(b2). They have good agreements with the numerical evolution of the two waves. Then, we change  $(\omega_0, \eta_p)$  into the diamond's coordinates  $(-4, 0.5)$  in Fig. 3(b1). Its amplitude evolution plot is shown in Fig. 3(b3). Before the appearance of second breathing period of KMB, the spontaneous oscillation emerges and breaks the generation of KMB, which indicates that the generation of KMB is not successful. The spontaneous oscillation always has a large influence on the generation of nonlinear waves, especially for the KMB generation. Although some efforts have been made to generate KMBs, generating a KMB with more than one breathing period from a nonideal initial perturbation is still an open problem.

Third, a periodic-localized perturbation can be used to generate MPS or TWB when the velocity matching is satisfied or not. Based on Eq. (9), one can derive

$$\begin{aligned} V_+^{(II)} &= \omega_0 + \frac{\beta_3}{6}(\omega_p^2 - 3\eta_p^2 + 3\omega_0^2) + \frac{\text{Im}[\sqrt{-P(4a_0^2 + P)}]}{2\omega_p}, \\ \Lambda_+^{(II)} &= \omega_0 + \frac{\beta_3}{6}(3\omega_p^2 - \eta_p^2 + 3\omega_0^2) - \frac{\text{Re}[\sqrt{-P(4a_0^2 + P)}]}{2\eta_p}, \end{aligned} \quad (17)$$

where  $P = (\eta_p - i\omega_p)^2(1 + \beta_3\omega_0)$ . When  $\omega_0 = 0$ , the distribution of  $|V_+^{(II)} - \Lambda_+^{(II)}|$  on  $\omega_p - \eta_p$  plane is shown in Fig. 3(c1). The colored ( $|V_+^{(II)} - \Lambda_+^{(II)}| > 0$ ) and white ( $|V_+^{(II)} - \Lambda_+^{(II)}| = 0$ ) regions respectively correspond to the generation of TWB and MPS. We set the initial parameters  $(\omega_p, \eta_p)$  as the triangle's coordinates in the plot. Its amplitude-evolution plot is shown in Fig. 3(c2). Despite the appearance of auto-modulation process, a MPS is generated with a negative velocity. On the localized envelope, many fringes can be observed and it can remain stable for a long distance. Then, we change  $(\omega_p, \eta_p)$  into the coordinates of the diamond in Fig. 3(c1). The amplitude-evolution plot is shown in Fig. 3(c3). Before the auto-modulation appears, a TWB is generated and propagates with a constant velocity. Compared with the MPS generation, the localized envelope and the

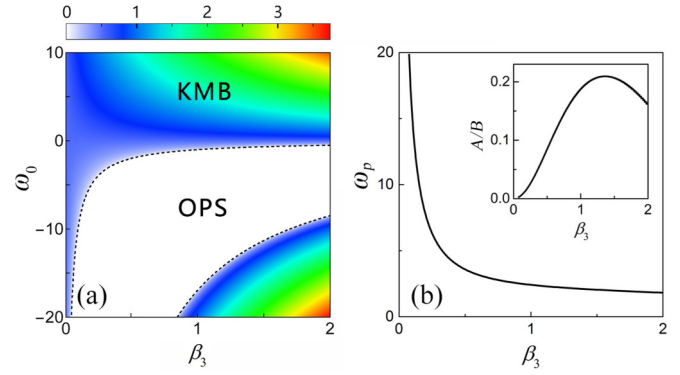


FIG. 4. (a)  $|K_{(t)}^{(II)}|$  value distribution on  $\beta_3 - \omega_0$  plane when  $\omega_p = 0$  and  $\eta_p = 0.5$ , where the white and colored regions denote OPS and KMB generation, respectively. (b) Generation condition of MPS on  $\beta_3 - \omega_p$  plane when  $\omega_0 = 0$ . The inset shows the dependence of the amplitude's asymmetric degree  $A/B$  on  $\beta_3$  for MPS generation.

fringe's velocities of generated TWB are obviously different, which matches well with our prediction. Note that Eqs. (14), (15), and (17) work only in the cases we consider here, so they need a recalculation when the parameter conditions are changed.

From the above results, the third-order dispersion has an influence on enriching the types of nonlinear waves. The generation condition of OPS and KMB when  $\omega_p = 0$  and  $\eta_p = 0.5$  is shown in Fig. 4(a). With  $\beta_3$  increasing, the required  $\omega_0$  for OPS generation is getting higher from a negative infinite value. When  $\beta_3$  approaches 0, the OPS generation is forbidden. The generation condition of MPS is also shown in Fig. 4(b) when  $\omega_0 = 0$ . With  $\beta_3$  increasing, the required  $\omega_p$  for MPS generation is getting lower. In the limit of  $\beta_3 \rightarrow 0$ , the required  $\omega_p$  has an unreachable infinite value. This result agrees well with the case of the NLS model. Meanwhile, the asymmetric degree of initial amplitude is defined by  $A/B$ , and its corresponding value for MPS generation is shown in the inset. The asymmetric degree increases from 0 and then decreases with  $\beta_3$  increasing, and it has a maximal value around 0.2. Its low asymmetric degree indicates the amplitude of component with frequency  $\omega_p$  is far less than the one with frequency  $-\omega_p$ . When  $\beta_3$  is close to 0, one can obtain  $A \rightarrow 0$ , which implies that the required perturbation for MPS generation has quasi-single frequency.

## V. EXPERIMENTAL FEASIBILITY OF MULTI- AND ONE-PEAK SOLITON EXCITATIONS

Now, we focus on the experimental feasibility for exciting multi- and one- peak solitons. By considering  $A = \sqrt{P_0}\psi$ ,  $T = [|\beta^{(2)}|/(\gamma P_0)]^{1/2}t$ , and  $Z = (\gamma P_0)^{-1}z$ , the model (1) can be transformed into a dimensional model. When the fiber loss is considered, the model is

$$iAZ - \frac{\beta^{(2)}}{2}A_{TT} - \frac{i\beta^{(3)}}{6}A_{TTT} + \gamma|A|^2A + i\frac{\alpha}{2}A = 0, \quad (18)$$

which describes the optical wave evolution in real fibers. Here,  $P_0$ ,  $\gamma$ ,  $\beta^{(2)}$ ,  $\beta^{(3)}$ , and  $\alpha$  scale respectively the input power, the nonlinearity, the group-velocity dispersion, the third-order dispersion, and the fiber loss. Here, we use the

experimental parameters of dispersion-shifted fiber used in Ref. [48]. The parameters are  $\beta^{(2)} = -0.86 \text{ ps}^2/\text{km}$ ,  $\beta^{(3)} = 0.12 \text{ ps}^3/\text{km}$ ,  $\gamma = 2.4 \text{ W}^{-1}\text{km}^{-1}$ ,  $\alpha = 0.2 \text{ dB/km}$ . The dimensionless coefficient of third-order dispersion is  $\beta_3 = (\gamma P_0/|\beta^{(2)}|^3)^{1/2}\beta^{(3)} = 0.0737$ . We change the input power  $P_0$  from  $0.63 \text{ W}$  into  $0.1 \text{ W}$  to weaken the symmetry-breaking phenomena. The initial condition is still the continuous wave perturbed by a sech-type envelope with two-frequency carrier waves,

$$A_p(0, T) = \sqrt{P_0} e^{i\Omega_0 T} [1 + (A_1 e^{i\Omega_p T} + A_2 e^{-i\Omega_p T}) \text{sech}(T/T_p)]. \quad (19)$$

The phase of the continuous wave is modulated periodically by the frequency  $\Omega_0$ . The relative periodicity and localization of the perturbation are scaled by the frequency  $\Omega_p$  and the half width  $T_p$ , respectively. When we consider the influence of random noise on wave excitations, the initial condition becomes

$$A_{\text{noise}}(0, T) = A_p(0, T)(1 + a_{\text{noise}} \text{Random}[-1, 1]), \quad (20)$$

where  $a_{\text{noise}}$  is the relative amplitude of random noise, and the function  $\text{Random}[a, b]$  can produce a random value between  $a$  and  $b$  at every numerical time point.

For the excitation of MPS, we set the background frequency  $f_0 = \Omega_0/2\pi = -840.769 \text{ GHz}$ , the perturbation frequency  $f_p = \Omega_p/2\pi = 555.988 \text{ GHz}$ , the half width  $T_p = 3.786 \text{ ps}$ , the perturbation amplitude  $A_1 = 0.03$ , and  $A_2 = 0.3$ , based on the analysis in the above sections. When  $a_{\text{noise}} = 0.001$ , the power-evolution plot is shown in Fig. 5(a). Its color scale denotes the normalized power,  $|A(Z, T)|^2/[P_0 \exp(-\alpha Z)]$ . One can see that a MPS propagating stably is excited. When the noise amplitude is increased, its profiles at the initial and final distances are compared in Figs. 5(b) and 5(c). The good agreement between them indicates that the MPS keeps robust against increased noise.

Then, we try the excitation of OPS. Since the initial perturbation is purely localized, the initial condition becomes

$$A_{loc}(0, T) = \sqrt{P_0} e^{i\Omega_0 T} [1 + A_{12} \text{sech}(T/T_p)]. \quad (21)$$

We set  $f_0 = \Omega_0/2\pi = -1140.8 \text{ GHz}$ ,  $T_p = 3.786 \text{ ps}$ , and  $A_{12} = 0.5$ . This set is located on the critical line between OPS and KMB regions [like in Fig. 3(b1)], which avoids the splitting of initial perturbation induced by wave feature's nondegeneration. Its power evolution plot is shown in Fig. 5(d) when  $a_{\text{noise}} = 0.001$ . A OPS propagates stably with a constant velocity. Its initial and final profiles are compared under different  $a_{\text{noise}}$  in Figs. 5(e) and 5(f). When  $a_{\text{noise}} = 0.01$ , small fluctuations appear, and the final profile agrees well with the initial one. When  $a_{\text{noise}} = 0.05$ , although the fluctuation in the final profile is amplified, the profile of soliton is still kept well. These results indicate that a MPS has a better robustness than a OPS when a noise is considered.

Note that diverse types of perturbations were used in real nonlinear fibers described by standard NLS model, and the types of them were similar to what we use [see Eqs. (19) and (21)]. For example, there were the cosine-type periodic perturbations [7, 11], the periodic perturbation with two frequency components [12], the purely localized one [49], and the periodic-localized one [9]. Specially, the spectral shaping

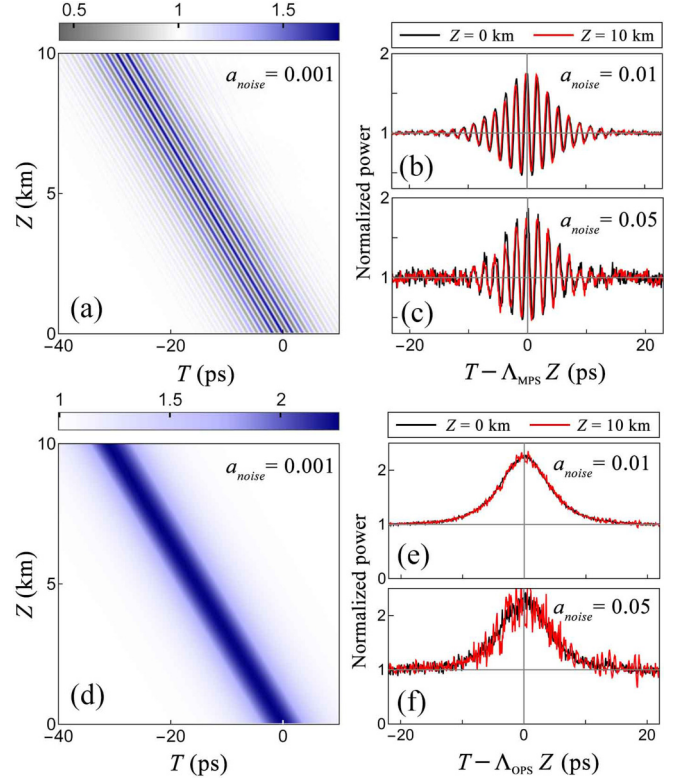


FIG. 5. (a) Power-evolution plot of MPS generation when  $a_{\text{noise}} = 0.001$ . (b) Its power profile at  $Z = 0 \text{ km}$  (black curve) and  $Z = 10 \text{ km}$  (red curve) when  $a_{\text{noise}} = 0.01$ . (c) The same as panel (b) except  $a_{\text{noise}} = 0.05$ . (d) Power-evolution plot of OPS generation when  $a_{\text{noise}} = 0.001$ . (e) Its power profile at  $Z = 0 \text{ km}$  (black curve) and  $Z = 10 \text{ km}$  (red curve) when  $a_{\text{noise}} = 0.01$ . (f) The same as panel (e) except  $a_{\text{noise}} = 0.05$ . The power mentioned here is the normalized power  $|A(Z, T)|^2/[P_0 \exp(-\alpha Z)]$ .  $\Lambda_{\text{MPS}}$  and  $\Lambda_{\text{OPS}}$  are the envelope velocities of MPS and OPS, respectively.

technology shown in Ref. [9] allows one to synthesize complex modulated initial conditions, which could contain various types of perturbations. It provides more possibility for preparing our initial conditions and implementing the corresponding generations of waves.

As an important and well-known effect in nonlinear fibers, the influence of Raman scattering on wave generations is necessary to be discussed. The Raman scattering is reflected by the nonlocal response function  $R_2(t)$  in the generalized NLSE, and its influence on instability gain can be analyzed by the standard LSA [50]. But it is difficult to apply the modified LSA to this model for wave features, due to the presence of nonlocal term. We note that the width of our pulses is much larger than  $100 \text{ fs}$ , so one can approximate the nonlocal Raman effect as the local one [23]. The nonlinear terms in Eq. (18) become  $\gamma(|A|^2 A - \tau_R |A|_T^2 A)$ , where  $\tau_R$  is the coefficient of Raman effect. Considering that the value of  $\tau_R$  was not provided in Ref. [48], we try the set  $\tau_R = 5 \text{ fs}$  in Ref. [51]. Its dimensionless coefficient is  $\tau_r = \tau_R(\gamma P_0/|\beta^{(2)}|)^{1/2} = 0.00264$ . From our analysis, the Raman scattering could lead to the “nondegeneration” of wave features when  $t \rightarrow +\infty$  and  $-\infty$ . So a wave could possess two different values of velocity on the left and right sides,

corresponding to the broadening or narrowing of waves in the numerical results. However, these phenomena happen observably only when the Raman scattering is much stronger than the experimental one we consider. In the cases we discuss, there is no obvious change between the soliton evolutions before and after the Raman scattering is considered. These results coincide with the statement in Ref. [48] that the Raman scattering can be neglected in the case we discuss because the continuous-wave power is far below the calculated Raman threshold (about 5 W).

## VI. CONCLUSION

In conclusion, we numerically generate six kinds of nonlinear waves and control their type, velocities, periodicity, and localization in the NLS model with third-order dispersion.

The generation condition of these waves is illustrated by means of the modified linear stability analysis method. They are generated from a periodic initial perturbation with a sech-type envelope on continuous waves. The velocities of their localized envelope and fringes are predicted successfully. Besides, the introduction of third-order dispersion is found to admit the generation of OPS and MPS so rich the kinds of waves. The results can provide the guidance for wave generations in real optical fibers and other nonlinear systems, like Bose-Einstein condensates, water, and plasmas.

## ACKNOWLEDGMENT

This work was supported by National Natural Science Foundation of China (Contacts No. 11875220 and No. 12047502).

- 
- [1] L. F. Mollenauer, R. H. Stolen, and J. P. Gordon, *Phys. Rev. Lett.* **45**, 1095 (1980).
- [2] R. H. Stolen, L. F. Mollenauer, and W. J. Tomlinson, *Opt. Lett.* **8**, 186 (1983).
- [3] L. F. Mollenauer, R. H. Stolen, J. P. Gordon, and W. J. Tomlinson, *Opt. Lett.* **8**, 289 (1983).
- [4] P. Emplit, J. P. Hamaide, F. Reynaud, C. Froehly, and A. Barthelemy, *Opt. Commun.* **62**, 374 (1987).
- [5] D. Krökel, N. J. Halas, G. Giuliani, and D. Grischkowsky, *Phys. Rev. Lett.* **60**, 29 (1988).
- [6] A. M. Weiner, J. P. Heritage, R. J. Hawkins, R. N. Thurston, E. M. Kirschner, D. E. Leaird, and W. J. Tomlinson, *Phys. Rev. Lett.* **61**, 2445 (1988).
- [7] J. M. Dudley, G. Genty, F. Dias, B. Kibler, and N. Akhmediev, *Opt. Express* **17**, 21497 (2009).
- [8] B. Kibler, J. Fatome, C. Finot, G. Millot, G. Genty, B. Wetzel, N. Akhmediev, F. Dias, and J. M. Dudley, *Sci. Rep.* **2**, 463 (2012).
- [9] B. Kibler, A. Chabchoub, A. Gelash, N. Akhmediev, and V. E. Zakharov, *Phys. Rev. X* **5**, 041026 (2015).
- [10] G. Xu, A. Gelash, A. Chabchoub, V. Zakharov, and B. Kibler, *Phys. Rev. Lett.* **122**, 084101 (2019).
- [11] B. Kibler, J. Fatome, C. Finot, G. Millot, F. Dias, G. Genty, N. Akhmediev, and J. M. Dudley, *Nat. Phys.* **6**, 790 (2010).
- [12] B. Frisquet, B. Kibler, and G. Millot, *Phys. Rev. X* **3**, 041032 (2013).
- [13] V. E. Zakharov and A. B. Shabat, *Sov. Phys. JETP* **34**, 62 (1972).
- [14] E. A. Kuznetsov, *Sov. Phys. Dokl.* **22**, 507 (1977); Y. C. Ma, *Stud. Appl. Math.* **60**, 43 (1979).
- [15] D. H. Peregrine, *Austral. Math. Soc. Ser. B* **25**, 16 (1983).
- [16] N. Akhmediev and V. I. Korneev, *Theor. Math. Phys.* **69**, 1089 (1986).
- [17] M. Tajiri and Y. Watanabe, *Phys. Rev. E* **57**, 3510 (1998).
- [18] N. Akhmediev, A. Ankiewicz, and M. Taki, *Phys. Lett. A* **373**, 675 (2009).
- [19] N. Akhmediev, A. Ankiewicz, and J. M. Soto-Crespo, *Phys. Rev. E* **80**, 026601 (2009).
- [20] A. Ankiewicz, D. J. Kedziora, and N. Akhmediev, *Phys. Lett. A* **375**, 2782 (2011).
- [21] B. L. Guo, L. M. Ling, and Q. P. Liu, *Phys. Rev. E* **85**, 026607 (2012).
- [22] J. S. He, H. R. Zhang, L. H. Wang, K. Porsezian, and A. S. Fokas, *Phys. Rev. E* **87**, 052914 (2013).
- [23] G. P. Agrawal, *Nonlinear Fiber Optics* (Academic Press, New York, 2007).
- [24] P. G. Kevrekidis, D. J. Frantzeskakis, and R. Carretero-González, *Emergent Nonlinear Phenomena in Bose-Einstein Condensates: Theory and Experiment* (Springer, New York, 2008).
- [25] H. C. Yuen and B. M. Lake, *Phys. Fluids* **18**, 956 (1975).
- [26] B. M. Lake, H. C. Yuen, H. Rungaldier, and W. E. Ferguson, *J. Fluid Mech.* **83**, 49 (1977).
- [27] H. Bailung, S. K. Sharma, and Y. Nakamura, *Phys. Rev. Lett.* **107**, 255005 (2011).
- [28] R. Hirota, *J. Math. Phys.* **14**, 805 (1973).
- [29] N. Sasa and J. Satsuma, *J. Phys. Soc. Jpn.* **60**, 409 (1991).
- [30] A. Ankiewicz, D. J. Kedziora, A. Chowdury, U. Bandelow, and N. Akhmediev, *Phys. Rev. E* **93**, 012206 (2016).
- [31] A. Ankiewicz, J. M. Soto-Crespo, and N. Akhmediev, *Phys. Rev. E* **81**, 046602 (2010).
- [32] U. Bandelow and N. Akhmediev, *Phys. Rev. E* **86**, 026606 (2012).
- [33] Y. S. Tao and J. S. He, *Phys. Rev. E* **85**, 026601 (2012).
- [34] S. H. Chen, *Phys. Rev. E* **88**, 023202 (2013).
- [35] L. C. Zhao, S. C. Li, and L. M. Ling, *Phys. Rev. E* **89**, 023210 (2014).
- [36] T. Xu, M. Li, and L. Li, *Europhys. Lett.* **109**, 30006 (2015).
- [37] C. Liu, Z. Y. Yang, L. C. Zhao, and W. L. Yang, *Phys. Rev. E* **91**, 022904 (2015).
- [38] C. Liu, Z. Y. Yang, L. C. Zhao, L. Duan, G. Y. Yang, and W. L. Yang, *Phys. Rev. E* **94**, 042221 (2016).
- [39] L. C. Zhao, S. C. Li, and L. M. Ling, *Phys. Rev. E* **93**, 032215 (2016).
- [40] A. Ankiewicz and N. Akhmediev, *Phys. Rev. E* **96**, 012219 (2017).
- [41] L. C. Zhao and L. Ling, *J. Opt. Soc. Am. B* **33**, 850 (2016).
- [42] L. Duan, L. C. Zhao, W. H. Xu, C. Liu, Z. Y. Yang, and W. L. Yang, *Phys. Rev. E* **95**, 042212 (2017).
- [43] L. Duan, Z. Y. Yang, P. Gao, and W. L. Yang, *Phys. Rev. E* **99**, 012216 (2019).



- [44] P. Gao, C. Liu, L. C. Zhao, Z. Y. Yang, and W. L. Yang, *Phys. Rev. E* **102**, 022207 (2020).
- [45] M. Conforti, S. Li, G. Biondini, and S. Trillo, *Opt. Lett.* **43**, 5291 (2018).
- [46] C. Liu, Z. Y. Yang, and W. L. Yang, *Chaos* **28**, 083110 (2018).
- [47] C. Liu, Z. Y. Yang, W. L. Yang, and N. Akhmediev, *J. Opt. Soc. Am. B* **36**, 1294 (2019).
- [48] M. Droques, B. Barviau, A. Kudlinski, M. Taki, A. Boucon, T. Sylvestre, and A. Mussot, *Opt. Lett.* **36**, 1359 (2011).
- [49] A. E. Kraych, P. Suret, G. El, and S. Randoux, *Phys. Rev. Lett.* **122**, 054101 (2019).
- [50] P. B ejot, B. Kibler, E. Hertz, B. Lavorel, and O. Faucher, *Phys. Rev. A* **83**, 013830 (2011).
- [51] D. R. Solli, C. Ropers, P. Koonath, and B. Jalali, *Nature (London)* **450**, 1054 (2007).